Supplementary Table 1. X-ray data collection and refinement statistics

Data collection	
Beamline	BL17U1, SSRF
Space group	P 31 2 1
Cell dimensions (Å)	a=183.96 b=183.96 c=79.09
Angles (°)	α=90.00 β=90.00 γ=120.00
Resolution (Å)	159.3-2.55 (2.63-2.55)
Total number of reflections	988771 (81305)
Number of unique reflections	50306 (4625)
Completeness (%)	99.9 (99.9)
Average redundancy	19.7 (17.6)
Rmerge	0.059 (0.962)
I/sigma (I)	29.4 (3.5)
Wilson B factor (Å)	73.9
Refinement	
Resolution (Å)	60.22-2.55
Number of reflections	50008
RMSD bond lengths (Å)	0.006
RMSD bond angles (°)	0.914
R_{work} (%)	19.87
R_{free} (%)	21.88
Average B-factors of protein	94.06
Ramachandran plot (%)	
Favored	98.24
Allowed	1.76
Outliers	0.00

The values in parentheses refer to the highest-resolution shell.

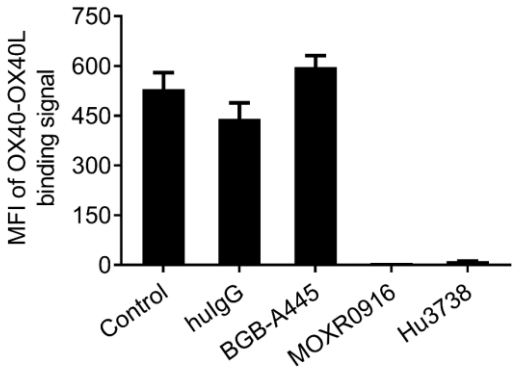

Supplementary Figure 1. Non–OX40L-blocking property of BGB-A445 in the cell-based assay and comparison with MOXR0916 and Hu3738. In this assay, the control was set as hOX40-mIgG2a alone, and the experimental groups included hOX40-mIgG2a in the presence of huIgG, BGB-A445 or reference antibodies. The data are presented as the mean value ± SD from three replicates.

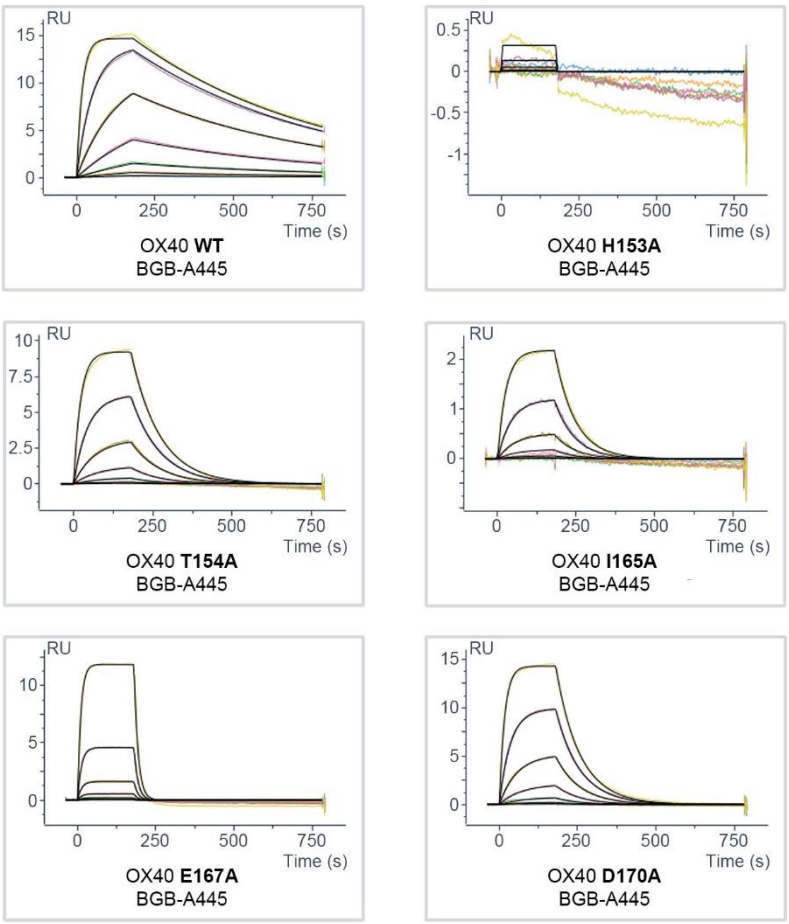

Protein	*ka* ($M^{-1}s^{-1}$)	*kd* (s^{-1})	K_D (M)	Mutant K_D/WT K_D
OX40 WT	$2.38 \pm 0.17 \times 10^{5}$	$1.68 \pm 0.02 \times 10^{-3}$	$7.09 \pm 0.48 \times 10^{-9}$	-
H153A	NA	NA	NA	NA
T154A	$1.85 \pm 0.18 \times 10^{5}$	$1.03 \pm 0.06 \times 10^{-2}$	$5.65 \pm 0.68 \times 10^{-8}$	8
I165A	$8.83 \pm 2.88 \times 10^{4}$	$1.55 \pm 0.11 \times 10^{-2}$	$1.96 \pm 0.83 \times 10^{-7}$	28
E167A	$8.50 \pm 2.01 \times 10^{4}$	$7.66 \pm 0.10 \times 10^{-2}$	$9.47 \pm 2.61 \times 10^{-7}$	134
D170A	$2.32 \pm 0.12 \times 10^{5}$	$1.33 \pm 0.06 \times 10^{-2}$	$5.72 \pm 0.05 \times 10^{-8}$	8

Supplementary Figure 2. SPR profiles of the activity of BGB-A445 against WT and mutant OX40 in the epitope mapping study. The graph (top) for each variant presented here is representative of four independent experiments with similar results, while the binding kinetics parameters for the variants (bottom) are presented as the means ± SDs of the results for the four replicates. NA, not applicable (the binding kinetics of BGB-A445 with the OX40 H153A mutant could not be accurately calculated because no significant binding signal was detected during SPR analysis). RU, responsive units.

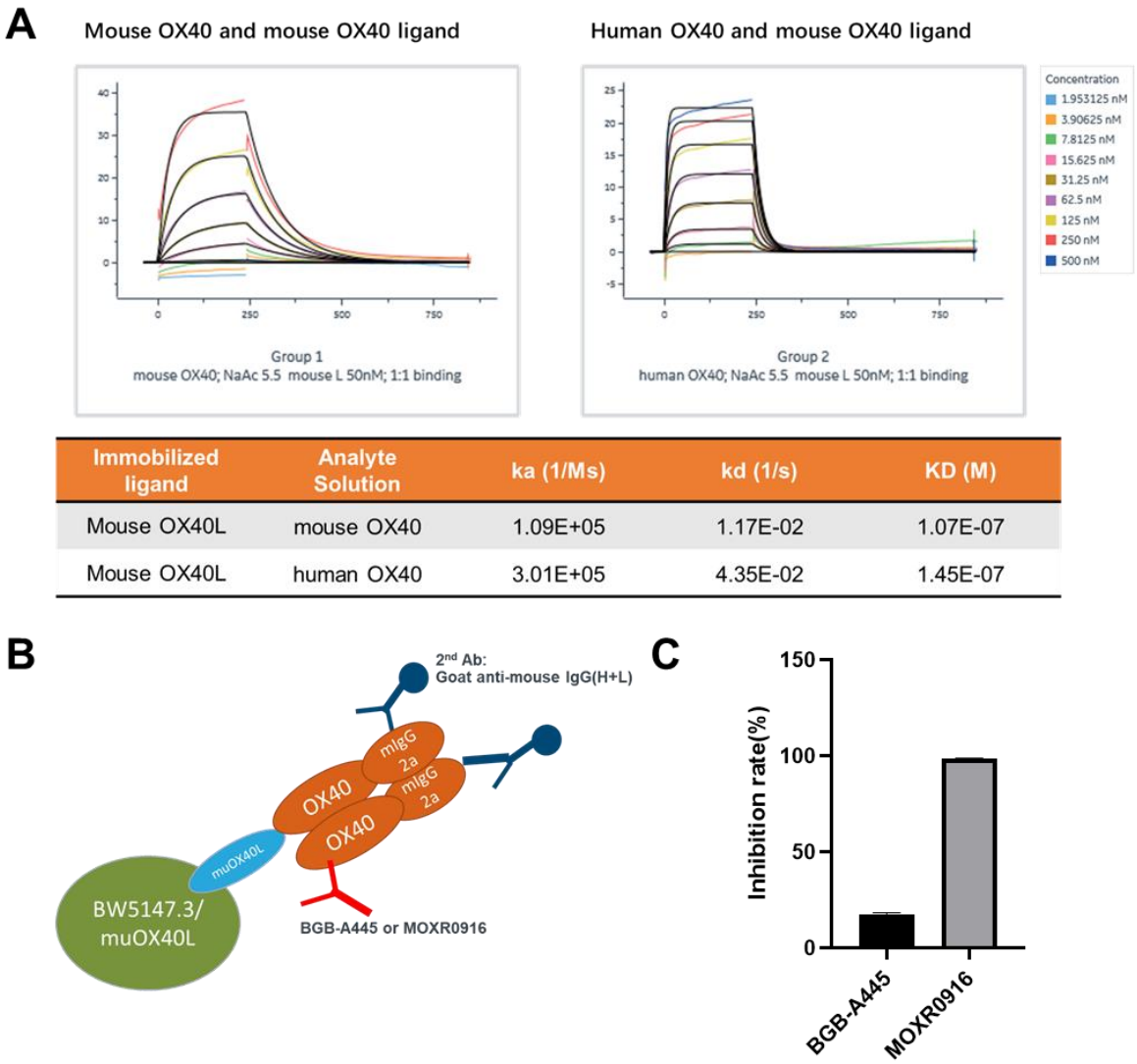

Immobilized ligand	Analyte Solution	ka (1/Ms)	kd (1/s)	KD (M)
Mouse OX40L	mouse OX40	1.09E+05	1.17E-02	1.07E-07
Mouse OX40L	human OX40	3.01E+05	4.35E-02	1.45E-07

Supplementary Figure 3. Human OX40 can bind to mouse OX40 ligand. (A) SPR profiles of mouse OX40 ligand binding to mouse and human OX40. The graph (top) is for mouse and human OX40 binding to mouse OX40 ligand, while the binding kinetics parameters (bottom) is present in the table. (B-C) Competition FACS assay of BGB-A445 and MOXR0916 using muOX40L expressing cell line and hOX40-mIgG2a Fc tag. The inhibition rate of the two antibodies were calculated. The data are presented as the mean value ± SD from two replicates.

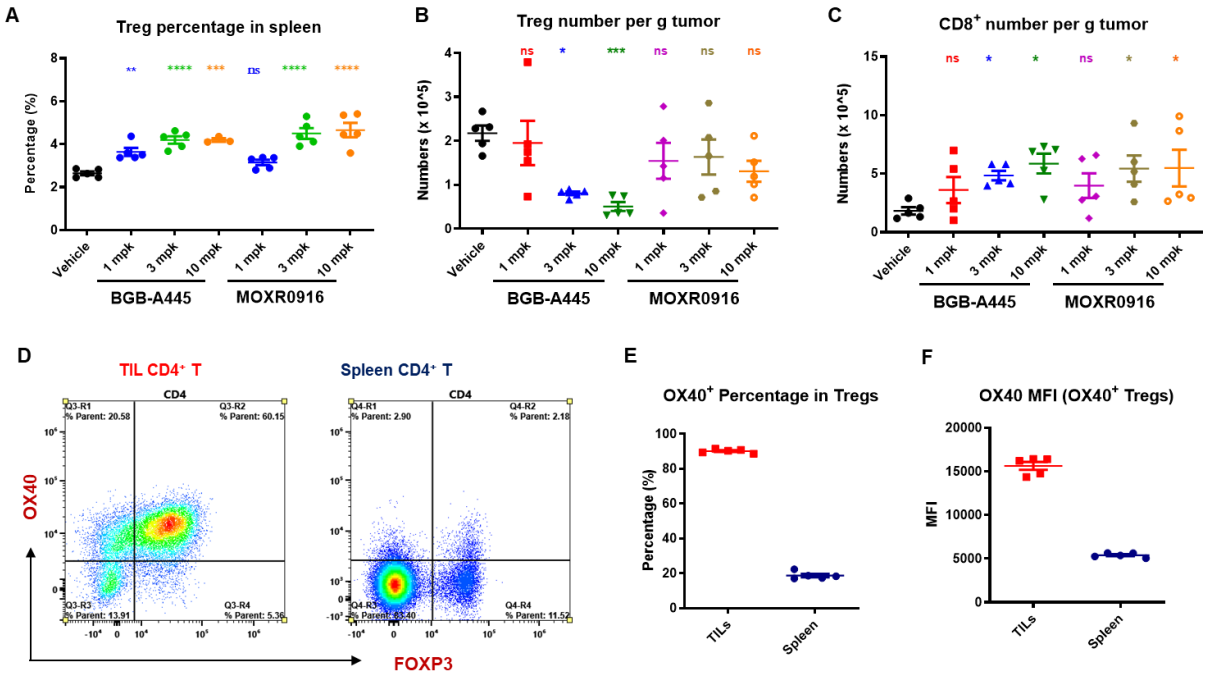

Supplementary Figure 4. BGB-A445 preferentially depletes Tregs in vivo. Twenty-four hours after the second injection of BGB-A445 or MOXR0916, tumors were isolated. Tumor infiltrated lymphocytes (TILs, $CD45^+$ cells) isolated from tumor-dissociated single-cell suspensions were stained and analyzed by flow cytometry. Treg percentage in the spleen (A), absolute number of Tregs (B) and $CD8^+$ T cells (C) per g tumor was calculate. All data are presented as the mean ± SEM, and each dot represents one animal. Statistical differences were analyzed using one-way ANOVA on log-transformed data using Holm-Sidak's multiple comparisons test (*, $p<0.05$, **, $p < 0.01$, ***, $p < 0.001$, ****, $p < 0.0001$). (**D**) Representative FACS results of OX40 expression on Tregs from TILs (isolated from tumors) or spleen tissue. (**E**) Percentage of OX40-expressing Tregs from TILs or spleen tissue. (**F**) OX40 expression level (calculated by MFI) on Tregs from TILs or spleen tissue. All data are presented as the mean, and each dot represents one animal.

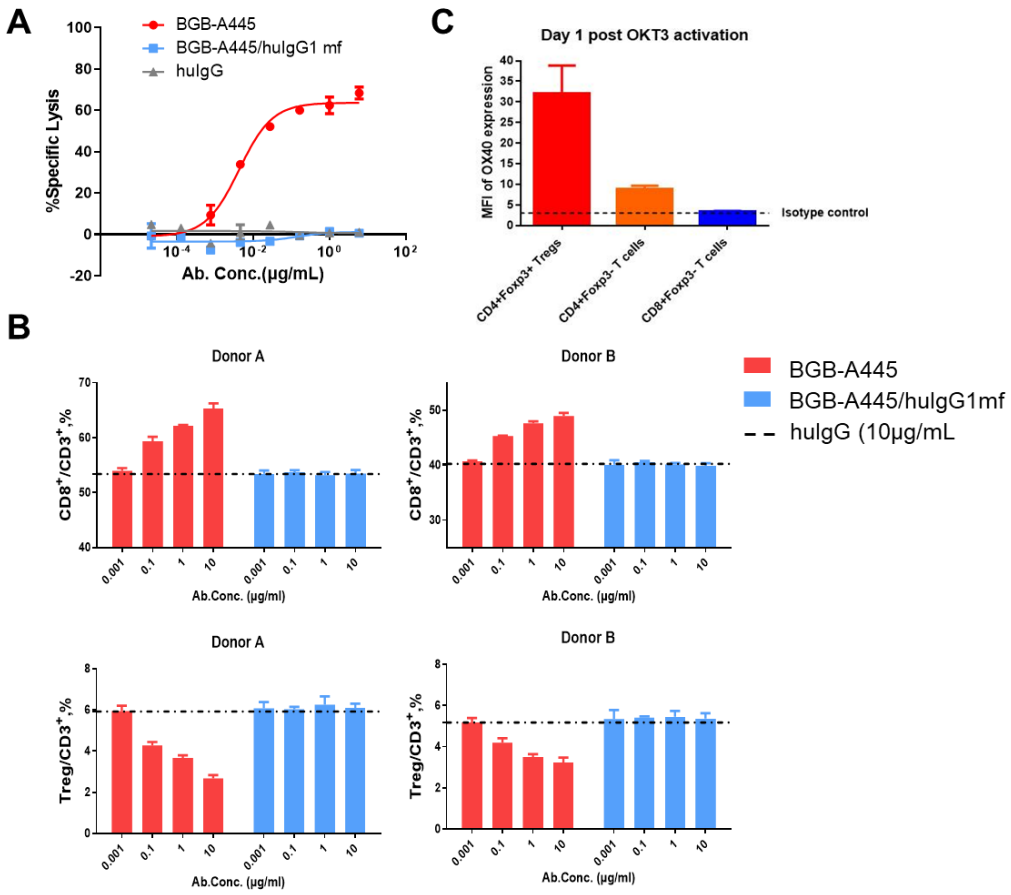

Supplementary Figure 5. BGB-A445 induces potent ADCC against OX40^{Hi} target BW/OX40 and Treg, while no effect on CD8^{+} cells. (**A**) To determine whether BGB-A445 could induce ADCC, a stable NK cell line (NK92MI/CD16V) expressing CD16 was used as an effector. BW/OX40 cells were used as target cells. The effector cells (E), NK92MI/CD16V, were co-cultured with target cells (T), BW/OX40, at an E:T ratio of 1 in the presence of BGB-A445 (0.00002-6 μg/mL) for 5h. Human IgG was used as a negative control. Cytotoxicity of NK92MI/CD16V cells against BW/OX40 cells was determined by the lactate dehydrogenase release assay. (**B)** NK92MI/CD16V cells were co-cultured with PHA-stimulated human PBMCs plus BGB-A445 for 18h and the percentage of CD8+ and Treg cells in T cells were determined by flow cytometry. (**C**) OX40 expression level on CD4, CD8 and Treg cells in human PBMCs stimulated with OKT3.